Title: Structural Basis for Antibody Neutralization of Pertussis Toxin

Authors: Jory A. Goldsmith[1], Annalee W. Nguyen[2], Rebecca E. Wilen[2], Wassana Wijagkanalan[3], Jason S. McLellan[1], Jennifer A. Maynard[2]

Affiliations:

[1] Department of Molecular Biosciences, The University of Texas at Austin, Austin, Texas, USA 78712

[2] Department of Chemical Engineering, The University of Texas at Austin, Austin, Texas, USA 78712

[3] BioNet Asia Co. Ltd., Prakanong, Bangkok, Thailand.

*Correspondence: maynard@che.utexas.edu (J.A.M), jmclellan@austin.utexas.edu (J.S.M.)

SIGNIFICANCE

Antibodies neutralizing pertussis toxin (PT) prevent the severe clinical symptoms associated with infection by *Bordetella pertussis*. However, the molecular basis of effective PT-targeted immunity is poorly understood. To gain insight into PT-inhibitory mechanisms, we determined the cryo-electron microscopy structure of genetically detoxified PT (PTg) with two potently neutralizing antibodies to precisely define their epitopes. Carbohydrate-binding studies show that the hu11E6-binding surface on PT interacts with N-linked glycans and that blocking these interactions prevents PT's T cell mitogenic activities. Hu1B7 binds an epitope near the S1 active site that includes S5 contacts but these do not appear important for neutralization. This work identifies PT-neutralizing epitopes and supports inclusion of the hu1B7 and hu11E6 epitopes in next-generation vaccines and PT-based immunogens.

SUMMARY/ABSTRACT

Pertussis toxin (PT) is a key protective antigen in vaccine- and natural immunity-mediated protection from *Bordetella pertussis* infection. Despite its importance, no PT-neutralizing epitopes have been characterized structurally. To define neutralizing epitopes and identify key structural elements to preserve during PT antigen design, we determined a 3.6 Å cryo-electron microscopy structure of genetically detoxified PT (PTg) bound to hu11E6 and hu1B7, two potently neutralizing anti-PT antibodies with complementary mechanisms: disruption of toxin adhesion to cells and intracellular activities, respectively. Hu11E6 bound the paralogous S2 and S3 subunits of PTg via a conserved epitope, but surprisingly did not span the sialic acid binding site implicated in toxin adhesion. High-throughput glycan array analysis showed that hu11E6 specifically prevents PTg binding to sialylated N-glycans, while a T cell activation assay showed that hu11E6 blocks PTg mitogenic activities to define the neutralizing mechanism. Hu1B7 bound a quaternary epitope spanning the S1 and S5 subunits, although functional studies of hu1B7 variants suggested that S5 binding is not involved in its PT neutralization mechanism. These results are the first to structurally define neutralizing epitopes on PT, improving our molecular understanding of immune protection from *B. pertussis* and providing key information for the future development of PT immunogens.

1   **INTRODUCTION**

2   *Bordetella pertussis,* the common respiratory pathogen and causative agent of whooping cough,

3   continues to be responsible for ~1% of global childhood mortality despite the wide availability of

4   effective vaccines [1]. Development of inactivated whole-cell pertussis vaccines (wP) decreased the

5   annual U.S. case load from over 150,000 in the 1930s to <5,000 in the 1970s. However, high lot-to-lot

6   variability and reactogenicity following vaccination with wP led to the subsequent development and

7   adoption of acellular vaccines (aP), which contain purified virulence factors such as pertussis toxin (PT),

8   filamentous hemagglutinin (FHA), type 2 and type 3 fimbriae (FIM2/3) and pertactin (PRN) [2].

9   The rising incidence of *B. pertussis* infection over the past two decades suggests that aP vaccines

10 may be less efficacious than wP vaccines [3]. Outbreaks in adolescents have been observed in populations

11 vaccinated with aP, suggesting that aP-induced immunity wanes rapidly and contributes to the current

12 large outbreaks across the UK and EU [4, 5]. In addition, the upregulation of PT and the loss of PRN

13 observed in clinical isolates suggest that circulating *B. pertussis* may adapt in response to selective

14 pressure imposed by vaccines [6]. To combat pertussis resurgence, improved acellular pertussis vaccines

15 are needed, but little is known about the protective epitopes on any pertussis vaccine antigen.

16   PT is secreted at high levels by *B. pertussis* during human infection and is a primary component

17 of all licensed acellular pertussis vaccines. Titers of PT-binding antibodies are predictive of recent

18 infection and high anti-PT titers correlate with less severe disease in humans [7, 8], although there is no

19 accepted serological correlate of protection [9]. In addition, experimental infection in the baboon model

20 indicates that PT-neutralizing antibodies are necessary and sufficient to block disease symptoms without

21 altering bacterial colonization [10][11]. Many currently circulating clinical isolates include the PTP3

22 promoter change that increases PT expression relative to isolates from previous decades [12], indicating

23 PT will continue to be a key target in future vaccines [2].

24   PT is a classic AB_5 toxin, with a catalytically active S1 (A) subunit that sits atop a donut-shaped

25 B_5 subunit. Five structural proteins combine to form the receptor-binding B subunit: the homologous S2

4

26   and S3 subunits, which each form heterodimers with S4, and then associate with S5 [13]. Binding to

27   sialylated glycoproteins on the target cell is mediated by carbohydrate-binding regions in the S2 and S3

28   domains [14, 15] and is followed by receptor-mediated endocytosis and retrograde transport of PT to the

29   ER [16]. Here, the reducing environment and presence of ATP causes S1 dissociation and transport out of

30   the ER by the ER-associated degradation (ERAD) system [17]. Once in the cytoplasm, S1 ADP-

31   ribosylates the alpha subunit of $G_{i/o}$ proteins to disrupt cellular signaling [18]. Phenotypically, PT exerts

32   various systemic effects, including histamine sensitization, islet activation, and leukocytosis [19].

33   While many studies have examined overall serological responses to PT, fewer have examined the

34   biochemical basis for toxin neutralization. Of the four characterized epitope groups on S1, just one is

35   potently neutralizing in all assays evaluated [20, 21]. Biochemical data suggest the prototypical protective

36   antibody hu1B7 binds an epitope spanning the S1 and B subunits near the active site to interfere with

37   intracellular toxin trafficking [22, 23]. The most protective B subunit antibody characterized, hu11E6,

38   appears to block receptor binding [23]. Since chemical detoxification of PT skews the immune response

39   to non-neutralizing B subunit epitopes [24, 25] and reduces binding by hu1B7, hu11E6 and other

40   neutralizing antibodies [26, 27], genetically detoxified PTg variants such as the R9K and G129E variants

41   [28] and C180 fragment of S1 [29, 30] are attracting interest for next-generation vaccines. However, no

42   structural data are available for the PT-binding antibodies to define epitopes that merit preservation

43   during antigen engineering.

44   To gain insight into their inhibitory mechanisms, we sought to define the structural basis for PT-

45   binding by neutralizing antibodies. Using cryo-EM, we determined a high-resolution structure of PTg in

46   complex with the hu1B7 and hu11E6 Fabs, which exhibit synergistic protection in multiple murine and

47   baboon models of disease [10, 31, 32]. Delineation of the key epitopes targeted by hu1B7 and hu11E6

48   will support use of these antibodies as serological probes, allow for tracking of escape mutations in

49   circulating strains and guide the production of next-generation PT vaccines.

50

51 **RESULTS**

52 **Cryo-EM structure of the PTg-hu1B7-hu11E6 complex**

53   To better understand the neutralizing mechanisms of hu1B7 and hu11E6, two of the most potent

54 and best-studied neutralizing antibodies against PT, we aimed to determine a cryo-EM structure of the

55 antigen-binding fragments (Fabs) of these antibodies in complex with PT. As one motivation behind

56 newly developed PTg antigens is preservation of neutralizing epitopes, we complexed the hu1B7 and

57 hu11E6 Fabs to a PTg antigen (R9K / E129G), which was produced in an engineered *B. pertussis* strain

58 [33]. The two amino acid changes in PTg do not appear to impact binding of the parental 1B7 and 11E6

59 antibodies to PT (Fig. S1).

60   To confirm the homogeneity of the PTg preparation and complex formation, the PTg-hu1B7-

61 hu11E6 complex was analyzed by negative-stain electron microscopy (nsEM). Micrographs of PTg-

62 hu1B7-hu11E6 adsorbed to the carbon layer of CF-400Cu grids and stained with methylamine tungstate

63 exhibited homogeneous particle distribution (Fig. S2A). 2D class-averages of extracted particles

64 confirmed that PTg was binding to 2 or 3 Fab molecules (Fig. S2B).

65   To prepare samples for cryo-EM analysis, the PTg-hu1B7-hu11E6 complex was applied to

66 UltrAuFoil grids[34], which contain a holey gold film on a gold support, and subsequently blotted and

67 plunge-frozen using a Vitrobot Mark IV. Initial screening of grids prepared in this manner resulted in

68 heterogeneous particle distributions largely composed of aggregates or small particles that were either

69 excess Fab or dissociated complex (Fig. S3A). The particle homogeneity and lack of aggregation

70 observed in the nsEM images suggested that the heterogeneity observed in the cryo-EM images is specific

71 to the blotting and plunge-freezing process, and that the sample may have been denatured by the air-water

72 interface. The inclusion of detergents in cryo-EM samples can mitigate aggregation and other effects of

73 the air-water interface. Accordingly, we froze grids of PTg-hu1B7-hu11E6 containing 0.1% Amphipol

74 but observed a similar heterogeneous mixture of aggregate and dissociated particles on these grids (Fig.

75 S3B), similar to conditions lacking detergent (Fig. S3A). This prompted us to screen 3 additional

76 detergent conditions: 0.02% fluoro-octyl maltoside, 0.4% CHAPS, and 0.1% β-octyl glucoside. Grids

6

77 prepared with 0.4% CHAPS contained particles too small to be the PTg-hu1B7-hu11E6 complex and

78 were likely to be excess Fab or dissociated components of the complex (Fig. S3C). The grids prepared

79 with 0.04% fluoro-octyl maltoside contained very few particles within the holes, although they appear

80 intact (Fig. S3D). Notably, grids prepared with 0.1% β-octyl glucoside exhibited a homogeneous

81 population of particles, with little to no aggregate present (Fig S3E). This grid was therefore chosen for

82 cryo-EM data collection.

83   Before collecting a full dataset, *ab initio* reconstruction and homogeneous refinement were

84 performed on particles extracted from a test dataset containing 20 movies. The orientation distribution

85 plot for this reconstruction displayed extreme preferred orientation bias, with almost every particle

86 adopting the same pose (Fig. S3F). To mitigate the preferred orientation bias, the full dataset of 1,500

87 movies was collected with a stage tilt of 30º. After motion correction, CTF estimation, and particle

88 picking, 1,694,697 particle picks were extracted and subjected to multiple rounds of *ab initio*

89 reconstruction and heterogeneous refinement. A final stack of 316,937 particles was subjected to

90 homogeneous refinement to yield a 3.6 Å resolution reconstruction (Figs. 1A, S4, S5). Using the crystal

91 structure of PT (PDB ID: 1PRT) as a starting model, a model of the PTg-hu1B7-hu11E6 complex was

92 built into the map (Figs. 1B, S6).

93 **Hu11E6 binds to a conserved epitope in both S2 and S3 subunits of PT**

94   The paralogous PT S2 and S3 subunits share ~70% identity across two distinct domains: an N-

95 terminal aerolysin/pertussis toxin domain (APT) with similarities to C-type lectins and a C-terminal B-

96 subunit domain that supports toxin assembly. Despite this modest sequence identity, hu11E6 exhibits a

97 nearly identical binding mode towards S2 and S3 due to hu11E6 binding conserved residues on the APT

98 surface. The light chain (LC) of hu11E6 buries 391 Å^2 surface area on S3 and 370 Å^2 surface area on S2,

99 while the heavy chain (HC) of 11E6 buries 453 Å^2 surface area on S3 and 376 Å^2 surface area on S2. Ten

100 hydrogen bonds are formed between hu11E6 and S3 (Fig. 2, top), nine of which form in an identical

101 manner between hu11E6 and S2 (Fig. 2, bottom). The only hydrogen bond formed between hu11E6 and

102 S3 that is not formed between hu11E6 and S2 is between the mainchain carbonyl oxygen of hu11E6 HC

103   Asn56 and the sidechain amide nitrogen of Gln182 (Fig. 2, top). In S2, the homologous residue of S3

104   Gln182 is Glu182, which cannot form the same hydrogen bond with the mainchain carbonyl oxygen of

105   hu11E6 HC Asn56.

106   Previously, in an attempt to determine the binding site for its carbohydrate receptor, PT was

107   crystallized in the presence of an 11-mer oligosaccharide, of which the terminal two residues (mannose

108   and sialic acid) were resolved bound to S2 and S3 [35]. Critically, these previously observed sialic acid

109   binding sites do not overlap with the hu11E6-binding sites, but are ~15–20Å away on the same face of the

110   S2 or S3 subunit (Fig. 3A). It is notable that this face is largely conserved between S2 and S3, with sialic

111   acid and hu11E6 both binding to conserved patches (Fig. 3B). By contrast, the bottom face of S2/S3 (180º

112   opposite the S1 subunit) is formed predominantly by residues that differ between S2 and S3. This

113   suggests that additional carbohydrate-binding sites, which are blocked by hu11E6 binding, are present on

114   the conserved face.

Inhibition of carbohydrate binding by hu11E6

116   To assess whether hu11E6 directly interferes with glycan recognition, we measured binding of

117   PTg to a high-throughput glycan array containing 562 carbohydrates in the presence and absence of the

118   hu11E6 Fab. PTg alone binds to sialylated N-glycans, asialo-N-glycans and other carbohydrates (such as

119   the sialyl Lewis[X] blood group antigen (Neu5Acα2-3Galβ1-4(Fucα1-3)GlcNAc) and c-series ganglioside

120   GQ2 (Neu5Acα2-8Neu5Acα2-8Neu5Acα2-8Neu5Acα2-3(GalNAcβ1-4)Galβ1-4Glcβ; Figure 4A-D).

121   This is similar to a previous glycan array study of PT that demonstrated interactions with 4 major

122   carbohydrates or carbohydrate classes [36]: 1) sialylated N-glycans, 2) asialo-N-glycans, 3) compounds

123   with a terminal Sialo-2,3-lactose, with the strongest hit in this group being sialyl Lewis[X] and 4) polysialic

124   acid compounds, with the strongest hit in this group being the GQ2. However, when first complexed to

125   hu11E6 Fab, no PTg binding to sialylated N-linked glycans was observed (Figure 4A, 4B). Hu11E6 also

126   reduced binding to some asialo-N-glycans (Figure 4A, 4C) while other carbohydrate hits were unaffected,

127   including the sialyl Lewis[X] and GQ2 (Figure 4A, 4D). Together, this suggests that hu11E6 blocks an N-

128   linked glycan recognition site in the N-terminal APT domain of S2/S3, whereas additional sites, likely in

129   the C-terminal B-subunit domain, were not blocked.

130   Previous studies demonstrated PT activation of T cell signaling in an antigen-independent manner

131   leading to T cell anergy, exhaustion, and apoptosis, which is mediated by B-subunit interactions with a

132   receptor thought to be closely associated with or in the TCR complex [37]. To determine whether hu11E6

133   blockade of PTg–sugar interactions would also diminish T cell activation, we performed an activation

134   assay with PTg, the Fabs of hu1B7, hu11E6 or an isotype control and peripheral blood mononuclear cells

135   (PBMCs) (Fig. 4E). Briefly, PTg was preincubated with serially diluted Fab, then co-incubated overnight

136   with isolated human donor PBMCs, before using flow cytometry to quantify the percent of activated

137   CD3-positive T cells using CD69-upregulation as an activation marker (Fig. S7A). Serially diluted PTg

138   indicated that 9.5 nM induced strong activation and this concentration was selected for antibody

139   inhibition experiments (Fig S7B). Whereas cells incubated with PT and the isotype control showed a high

140   level of T cell activation (~90% at all antibody concentrations), this was slightly reduced by hu1B7

141   (~70% at >10 nM), while hu11E6 showed a nearly complete knockdown of PTg stimulation at higher

142   antibody concentrations (~5% at 100 nM) and a 50% inhibitory concentration (IC_{50}) of 24.5 ± 2.5 nM.

143   This indicates that hu11E6 is not only capable of blocking activities mediated by the PT A subunit, but

144   also those mediated by the B subunit [31].

145

146   **Hu1B7 binds to a quaternary epitope that spans S1 and S5**

147   In the PTg-hu1B7-hu11E6 complex cryo-EM structure, the hu1B7 heavy chain and light chain

148   bury 428 $Å^2$ and 359 $Å^2$, respectively, of solvent-accessible surface area on PTg (Fig. 5A, B). Consistent

149   with epitope mapping studies, the hu1B7 light chain (LC) Phe32, Tyr49, Leu50, Trp91 and hu1B7 heavy

150   chain (HC) Ala99 form a hydrophobic interface on the surface of the PTg S1 β-sheet formed by β4, β8

151   and β9, contacting PT S1 Thr81, His83, Ile85, Tyr148 and Ile152 (Fig. 5C). Similarly, hu1B7 HC Trp33

152   packs onto the PTg S1 α3–β4 loop, and hu1B7 HC Asn50 and Ser97 form hydrogen bonds with PTg S1

153   Glu75 and Gly78 within this loop, respectively (Fig. 5D). In addition, hu1B7 heavy chain Ser56 forms a

9

154 hydrogen-bond between its sidechain oxygen and the C-terminal carboxyl group of S1 Glu99 (Fig. 5D).

155 Biochemical data have previously shown that hu1B7 interacts with PT S1 [24], with residue-level epitope

156 mapping suggesting the involvement of the loops approximately at S1 residues 77–84 (α3–β4 loop) and

157 149–155 (β8–β9 loop) [22, 38]. C

158   One possible mechanism of inhibition for hu1B7 is the inhibition of S1 catalytic activity. Hu1B7

159 binding to PTg does not alter the S1 conformation, and the α-carbons of hu1B7-bound S1 align to

160 unbound S1 [13] with an RMSD of 1.04 Å^2 (Fig. S8A). However, the active conformation of S1 that

161 binds NAD^+ contains an active-site cleft that is more closed relative to S1 in the B-oligomer (Fig. S8B).

162 Specifically, α3 moves inwards towards the cleft, positioning the substrate-binding residues Tyr59 and

163 Tyr63 for NAD^+ binding (Fig. S8B) [39]. Since hu1B7 binds to α3, it could allosterically prevent the

164 helix motion necessary to position Tyr59 and Tyr63 for substrate binding. Alternatively, hu1B7 could

165 inhibit binding of the Gαi substrate. Since the loop containing S1 residues 112–127 is involved in Gαi

166 binding in related toxins [39, 40], and is located on the opposite end of the active-site cleft as hu1B7 (Fig.

167 S8C), this seems unlikely. However, if Gαi occupies a large volume in the active site cleft, hu1B7 could

168 introduce steric clashes resulting in neutralization.

169   Unexpectedly, the hu1B7 heavy chain forms multiple contacts with PTg S5. Overall, the hu1B7

170 HC buries 262 Å^2 and 166 Å^2 on S1 and S5, respectively. hu1B7 HC Gly53 may also form a hydrogen

171 bond with PTg S4a Lys92, but the map is not well-resolved in this region (Fig. 5E, Fig. S6), leaving the

172 exact sidechain rotamer of PTg S4a Lys92 uncertain. Hu1B7 HC Gln61 and Gln64 form hydrogen bonds

173 with the sidechain oxygen and mainchain oxygen, respectively, of S5 Ser33, with hu1B7 HC Gln64

174 packing onto S5 Met32 and S5 Arg35 (Fig. 5F). Hu1B7 LC His94 packs onto S1 Arg79, which itself

175 forms a π–π stacking interaction with S5 Tyr97 as part of the interaction between S1 and the B-oligomer

176 (Fig. 5F). While hu1B7 light chain His94 does not directly bind S5, it may stabilize the interaction

177 between S1 Arg79 and S5 Tyr97. Binding of hu1B7 to both S1 and S5 suggests that hu1B7 binding may

178 prevent S1 subunit dissociation from the B-oligomer. Although hu1B7 neutralization likely occurs via

179   inhibition of PT retrograde trafficking [23], we previously hypothesized that clamping the S1 subunit to

180   the B-oligomer via interactions with S5 could contribute to hu1B7 neutralization.

181   **Neutralization activity of hu1B7 mutants**

182   To test whether clamping of S1 to S5 by hu1B7 contributes to the neutralization mechanism of

183   hu1B7, we generated an hu1B7 variant (hu1B7$_{mut}$) with point mutations expected to ablate the 3 hydrogen

184   bonds between hu1B7 and S5: S56A, Q61A, Q64A. If S1–S5 clamping were critical to the hu1B7

185   neutralization mechanism, then ablation of these hydrogen bonds would prevent neutralization. However,

186   hu1B7$_{mut}$ binding to PT, as measured by ELISA, and PT neutralization of CHO cell clustering, were not

187   detectably different from binding and neutralization by wild-type hu1B7 (Fig. S9). Therefore, S1–S5

188   clamping does not appear to play a role in hu1B7-mediated neutralization of PT.

189

190   **DISCUSSION**

191   All acellular pertussis vaccines evaluated to date aim to induce high titers of neutralizing

192   antibodies against PT since these mitigate the clinical symptoms of disease. This goal is complicated by

193   the chemical detoxification of PT in most current vaccines, a process that appears to alter the structure of

194   PT-neutralizing epitopes and their resulting immunogenicity. Characterization of key neutralizing

195   epitopes on PT will contribute to a mechanistic understanding of PT protection and allow for their

196   retention in future PT-based immunogens. Accordingly, we determined the structural basis for PT binding

197   and neutralization by two synergistic and potently neutralizing antibodies: hu11E6 and hu1B7.

198   Antibody hu11E6 binds the B subunit to block PT-glycan interactions required for cell binding

199   and toxicity. In the absence of antibodies, PT attachment to cells is mediated by the paralogous S2 and S3

200   subunits, which each contain two carbohydrate-binding domains: the N-terminal APT domain, which

201   resembles mammalian C-type lectins, and the C-terminal AB$_5$ toxin B-oligomer domain, which supports

202   B subunit assembly [15, 41, 42]. Hu11E6 binds an APT domain epitope that is almost perfectly conserved

11

203   across S2 and S3 (Fig. 3) and ablates PT interactions with sialylated N-glycans (Fig. 4B). This epitope

204   surprisingly does not overlap with the structurally defined sialic acid-binding site in the C-terminal B-

205   oligomer domain [13], nor does it affect binding to the sialyl Lewis[X] blood group antigen or GQ2

206   ganglioside, which contain 1 and 4 terminal sialic acid residues, respectively (Fig 4D). Since the S2/S3

207   subunits engage four glycan classes [36], this suggests that the C-terminal B-oligomer domain is likely

208   responsible for binding carbohydrates similar to Lewis[X] and GQ2 and that other sites on PT may bind

209   asialo-N-glycans. Overall, the N-terminal APT domain contains at least one binding site for a sialylated

210   N-linked glycan moiety critical for PT cell adhesion whose interactions are blocked by hu11E6 binding.

211   Hu11E6 blocks PT attachment to mouse spleen and CHO cells [23, 43], prevents PT activation of

212   human T cells (Fig. 4E) and is strongly protective in mouse infection models [31, 32, 44]. Mechanistic

213   studies have shown that PT triggers immediate TCR-mediated intracellular signaling in T cells by binding

214   an unknown receptor [37]. Here, we show that hu11E6 blocks this signaling and thus hu11E6-like

215   antibodies may provide protection against PT-mediated T cell anergy and exhaustion. However, hu11E6

216   only blocks binding by a fraction of the glycan species engaged by PT (Fig 4A-D). Therefore, binding of

217   sialylated N-glycans to the PT site blocked by hu11E6 represents a major attachment pathway *in vivo* but

218   PT may engage different glycans to target other cell types as occurs in other AB_5 toxins such as typhoid

219   toxin [45]. The importance of hu11E6-like antibodies in preventing T cell activation bolsters the rationale

220   for retaining B subunit epitopes in future PT immunogens.

221   Antibody hu1B7 prevents PT activity *in vitro* and potently protects infant baboons administered

222   an at-birth dose from infection six weeks later [10]. The hu1B7 epitope on PT is dominated by S1

223   interactions, with ~79% of the buried surface area on PT localized to S1 (Fig. 5). This is largely

224   consistent with previous biochemical studies: hu1B7 contacts defining the hydrophobic interaction with

225   S1 (L:W91, H:W33 and H: S97 with S1:H83 and Y148) and B-subunit interactions (L:H94 and S1:R79)

226   were correctly identified (Fig S5D,E) [22, 38]. In addition, Sutherland *et al*., correctly predicted

227   interactions with the B-oligomer based on decreased affinity of hu1B7 for recombinant S1 monomers.

12

228   However, the epitope was predicted to span the S1 and S4a subunits, whereas our structure shows the

229   epitope spanning S1 and S5, with just one S4a contact (Fig. S5E). Antibodies binding ricin toxin epitopes

230   that span the A-B toxin interface are also potently neutralizing [46], suggesting that this interface may be

231   a general site of vulnerability.

232   Protection by hu1B7 is more likely related to altered intracellular trafficking than direct inhibition

233   of catalytic activity. Access to the catalytic site is not impaired by hu1B7 binding although hu1B7-

234   induced conformational changes could allosterically inhibit binding of NAD+ or the Gαi substrate (Fig.

235   S8). Conversely, *in vitro* experiments with CHO cells suggested that hu1B7 alters PT intracellular

236   trafficking to mediate neutralization [23]. As S1 must dissociate from the B-oligomer to reach its eventual

237   target, one possibility is that hu1B7's quaternary epitope clamps S1 to S5, frustrating S1 dissociation.

238   Accordingly, we simultaneously ablated the three hydrogen bonds formed between hu1B7 and PT S5.

239   This had little effect on hu1B7 binding or neutralization (Fig. S9), suggesting that S1/S5 clamping is not

240   relevant for the hu1B7 neutralization mechanism. A second possibility is that hu1B7 disrupts interactions

241   required for PT retrograde trafficking. No mechanism has yet been described to mediate PT retrograde

242   transport, but multiple mechanisms have been described for other AB toxins, including a C-terminal

243   KDEL sequence for ER retention (cholera toxin), hitchhiking on a host protein that exhibits retrograde

244   transport (shiga toxin) [47] and interactions with ER-resident chaperones [48]. Mutagenesis of the hu1B7-

245   binding site could be used to generate non-binding probes to identify putative PT endosomal interaction

246   partners to define this mechanism.

247   Despite the success of PT as a vaccine antigen, the chemical detoxification process used to

248   inactivate PT in most approved aP formulations may have deleterious effects on antigenicity and

249   carbohydrate binding. The engineered PTg used in this work [33] was rendered inactive by introducing

250   R9K and E129G substitutions in the toxic S1 enzymatic subunit. Studies comparing PTd and PTg

251   immunogenicity in humans observed higher total neutralizing titers and more durable responses after

252   immunization with PTg-containing vaccines [28, 49, 50]; while sera from patients with confirmed

13

253   pertussis infection contained higher titers of antibodies binding specific neutralizing epitopes (including

254   the hu1B7 and hu11E6 epitopes) than sera from patients who recently received an acellular vaccination

255   containing PTd [26, 27]. Interestingly, glutaraldehyde inactivation entirely ablated binding to a model

256   sialylated N-glycan but only partially ablated binding to the asialylated version of the same carbohydrate

257   [51]. The similar impacts of hu11E6 binding and glutaraldehyde inactivation on glycan binding suggest

258   the same sialylated N-glycan site is affected. Therefore, intact carbohydrate sites on PTg likely represent

259   important neutralizing epitopes that risk loss during chemical inactivation. Since the PT and PTg crystal

260   structures are nearly identical (1.5 Å r.m.s.d.) [52], including in the hu1B7 and hu11E6 epitopes, this

261   indicates PTg may elicit more effective immune responses by preserving key surface epitopes.

262   Defining the structural basis for potent PT neutralization by hu11E6 and hu1B7 helps to explain

263   protection conferred by PT and will guide design of future PT immunogens. In addition, PT's complex

264   multi-subunit structure with unequal stoichiometry presents challenges for design of nucleic acid-based

265   vaccines. Development of simpler PT-like immunogens may require retention of S5 sequences to elicit

266   hu1B7-like antibodies and may benefit from focusing immune responses on the poorly antigenic S2/S3

267   subunits to elicit hu11E6-like antibodies. Together, this work supports the use of PTg over PTd in aP

268   vaccines and suggests immunogen design strategies to elicit high titers of potently neutralizing antibodies.

269

280

281   **AUTHOR CONTRIBUTIONS**

282   Conceptualization, J.A.G., J.A.M., and J.S.M.; Investigation and visualization, J.A.G., A.W.N.., R.E.W.;

283   Critical reagents, W.W.; Writing – Original Draft, J.A.M., J.A.G.; Writing – Reviewing & Editing, J.A.G,

284   A.W.N., R.E.W., W.W., J.A.M., and J.S.M.; Supervision, J.A.M. and J.S.M.

285

286   **DECLARATION OF INTERESTS**

287   J.A.M. has been awarded patent US20120244144, "Pertussis antibodies and uses thereof" (19 September

288   2011); J.A.M. and A.W.N. have been awarded patent US9512204B2 with Synthetic Biologics,

289   "Humanized pertussis antibodies and uses thereof" (6 December 2016) and filed "Stabilized pertussis

290   antibodies with extended half-life" (15 August 2017) with the U.S. Patent and Trademark Office. The

291   hu1B7 and hu11E6 antibodies were licensed to Synthetic Biologics (now Theriva). W.W. is an employee

292   of BioNet Asia, which produces and markets vaccines containing PTg.
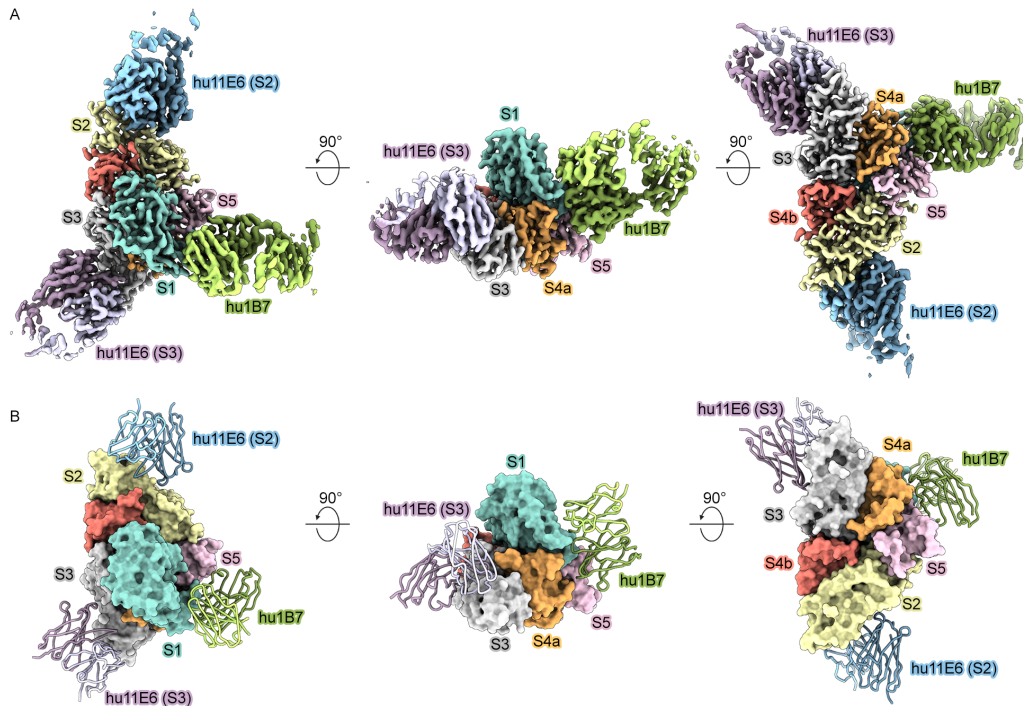
293

294

295

296

297

298

299

300

15

301   **FIGURES**

302

**Figure 1. Cryo-electron microscopy structure of PTg in complex with hu1B7 and hu11E6**

(A) Sharpened cryo-electron microscopy map of PTg+hu11E6+hu1B7 with S1 colored turquoise, S2

colored yellow, S3 colored white, S4a colored orange, S4b colored red, S5 colored pink, hu11E6 (S2)

colored blue, hu11E6 (S3) colored purple, and hu1B7 colored green. (B) Model of PTg+hu11E6+hu1B7

colored as in (A), with PTg subunits shown as molecular surfaces and hu11E6 (S2), hu11E6 (S3) and

hu1B7 shown as ribbon representations.
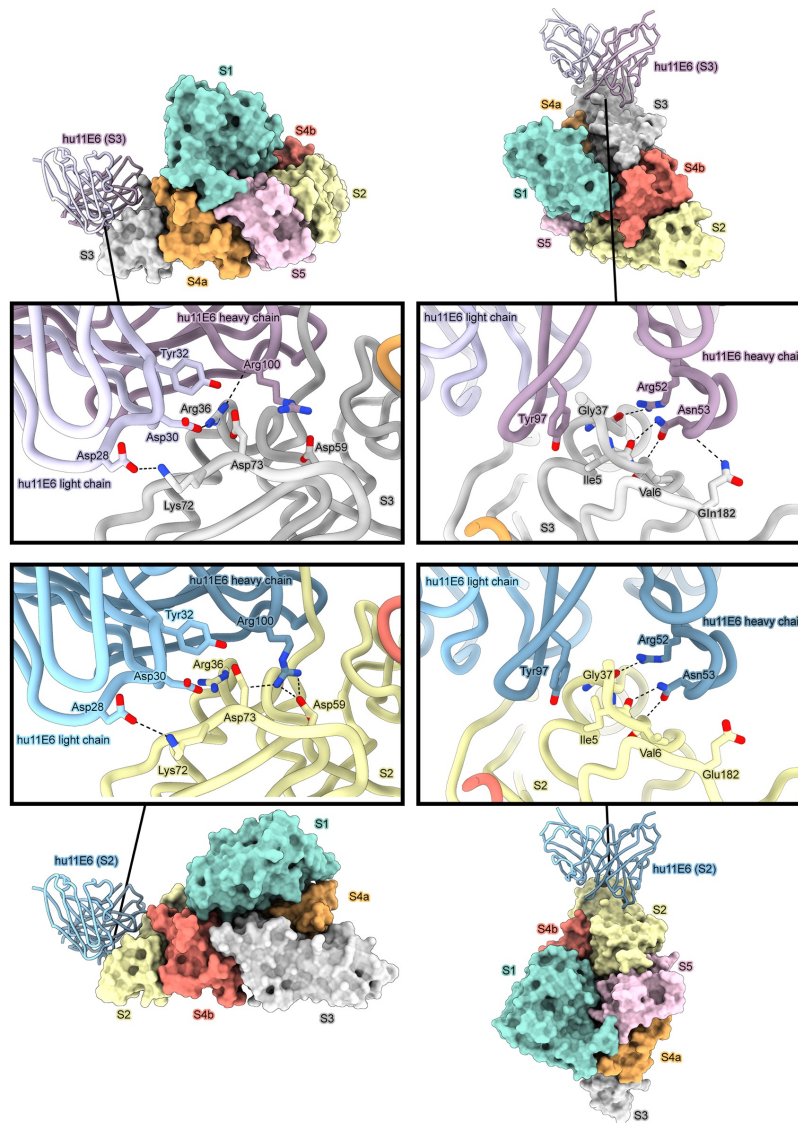
Figure 2. Hu11E6 binds to a conserved epitope on PTg S2 and S3

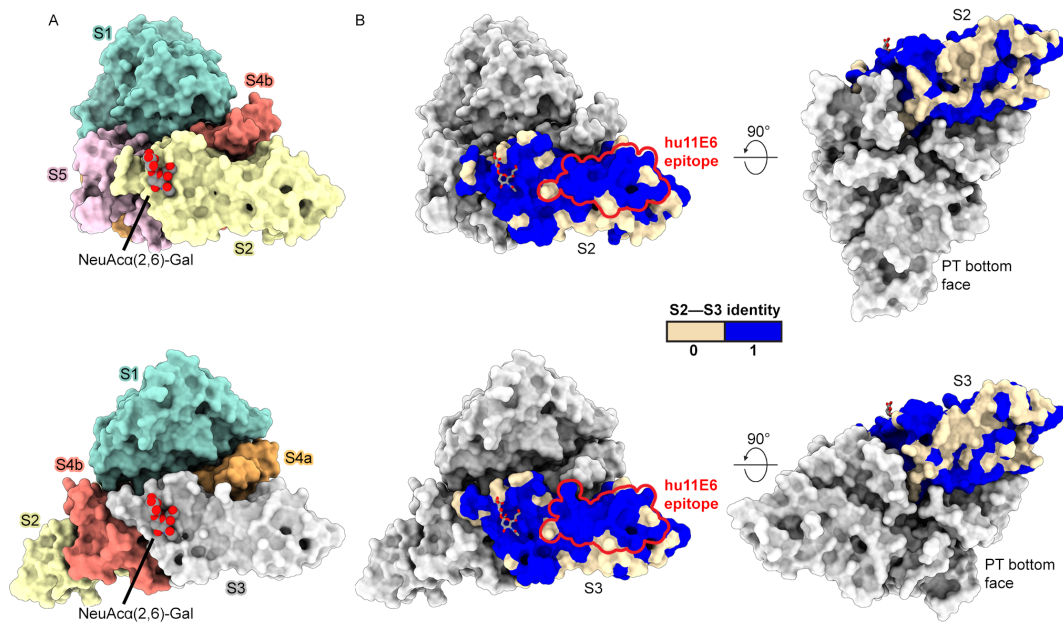Zoomed-out views of PTg bound to hu11E6 are shown with PTg as molecular surfaces, with S1 colored turquoise, S2 colored yellow, S3 colored white, S4a colored orange, S4b colored red, S5 colored pink, hu11E6 (S2) colored blue, hu11E6 (S3) colored purple, and hu1B7 colored green. hu11E6 is shown as a ribbon representation. The boxes show close-up views of the hu11E6 epitope on S3 (top) and S2 (bottom) subunits of PTg, with all proteins shown as ribbon representations and key interface residues shown as sticks.

Figure 3. Comparison of hu11E6 epitope and the known sialic acid binding site on PTg

(A) PTg shown as molecular surface with S1 colored turquoise, S2 colored yellow, S3 colored white, S4a colored orange, S4b colored red and S5 colored pink, with NeuAcα(2,6)-Gal disaccharide from PDB ID: 1PTO shown as molecular spheres with carbons colored gray and oxygens colored red. (B) PTg shown as a molecular surface with all subunits colored white and either S2 (left) or S3 (right) colored by per-residue S2–S3 identity, where shared residues between S2 and S3 are colored blue and residues that differ between S2 and S3 are colored tan. The outline of the hu11E6 epitope on S2 and S3 is shown in red. The NeuAcα(2,6)-Gal disaccharide described in (A) is shown on S2 and S3 using stick representation.

18
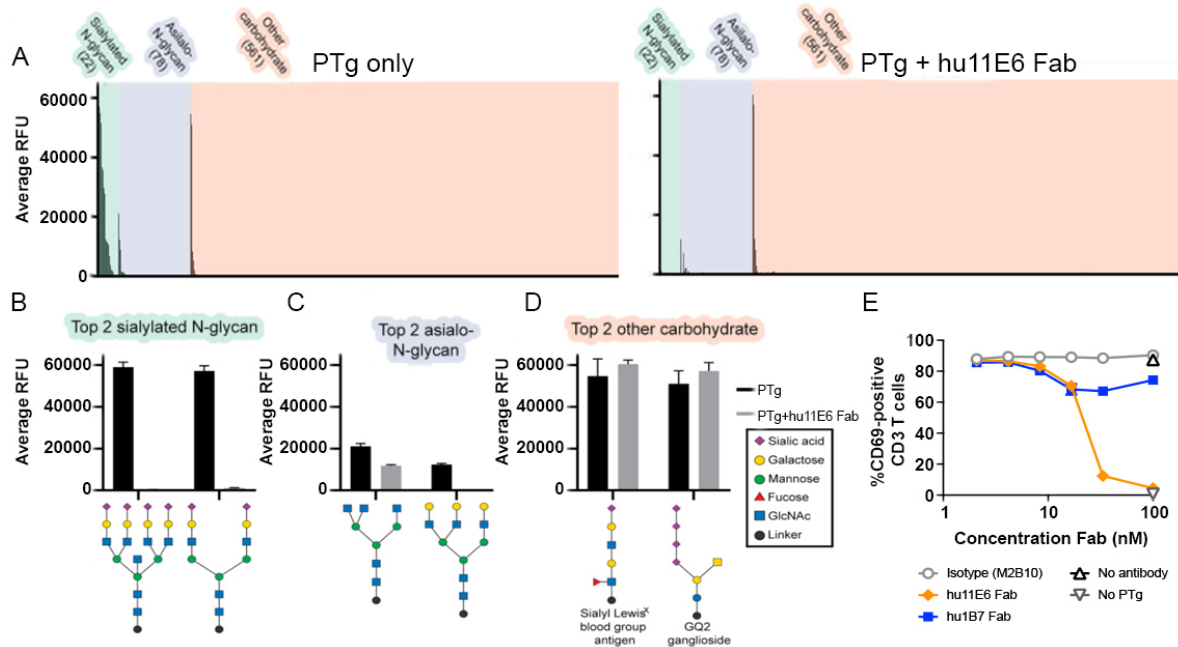
Figure 4. Hu11E6 prevents PTg binding to sialylated N-glycans and T-cell activation

(A) Summary of high-throughput carbohydrate-binding array results for PTg and PTg+hu11E6 Fab. Carbohydrates were separated into 3 groups: sialylated N-glycans (green), asialo-N-glycans (blue), and all other carbohydrates (coral). For PTg (top), carbohydrates were ranked with descending relative fluorescence units (RFU). For PTg+hu11E6 Fab (bottom), carbohydrates were ordered as for PTg alone. Close-up view of the RFU for PTg versus PTg+hu11E6 Fab for the top two (B) sialylated N-glycan hits, (C) asialo-N-glycan hits, and (D) other carbohydrate hits. (E) Antibody Fab inhibition of PTg-mediated T cell activation. Serially diluted Fabs were incubated with PTg and then human donor PBMCs overnight before using flow cytometry to measure the percent of activated, CD69-positive CD3+ T cells. Two-way ANOVA analysis used to determine significance; hu11E6 versus hu1B7 and hu11E6/ hu1B7 versus isotype comparisons indicated with **** reached $p<0.0001$. Data shown are representative of two biological replicates, with the average and range of two technical replicates shown.
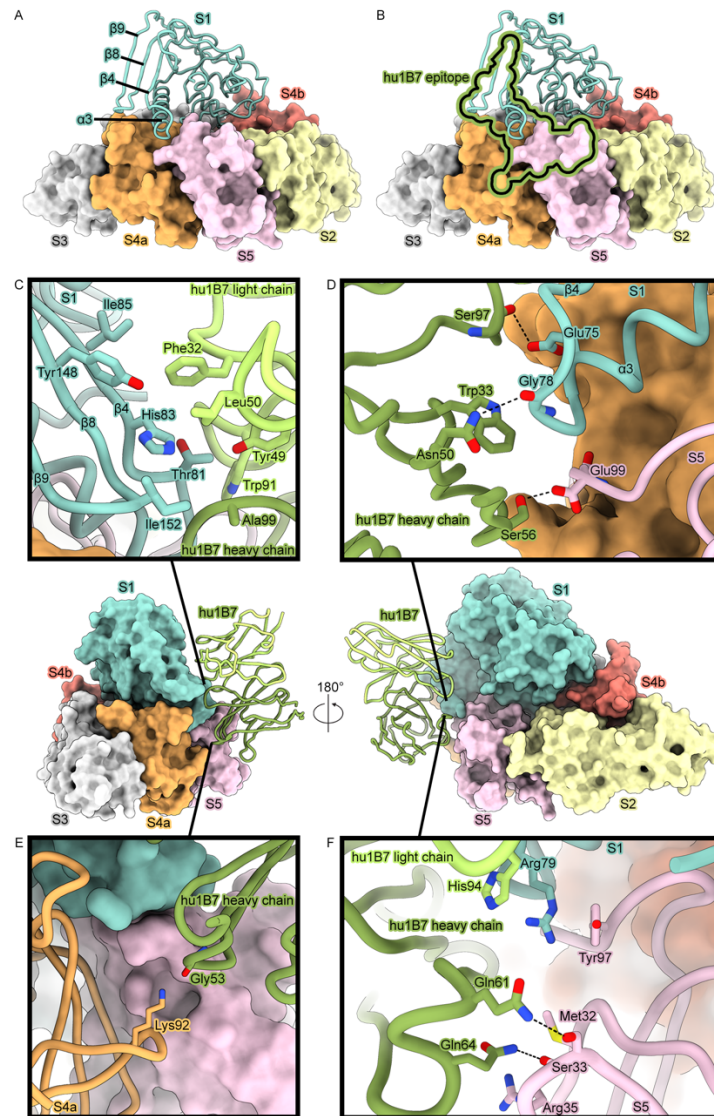
Figure 5. Hu1B7 binds a quaternary epitope spanning PTg S1 and S5

(A) PTg shown as molecular surfaces, with S1 colored turquoise, S2 colored yellow, S3 colored white, S4a colored orange, S4b colored red, S5 colored pink, hu11E6 (S2) colored blue, hu11E6 (S3) colored purple, and hu1B7 colored green. α3, β4, β8 and β9 secondary structural elements are labeled on S1. (B) Same as (A), with the outline of the hu1B7 epitope shown in black with a green outline. (C,D,E,F) Views of PTg bound to hu1B7 are shown in the middle row. Boxes show zoomed views depicting ribbon representations of hu1B7 and either S1 (C), S1 and S5 (D,F) or S4a (E), with key interface residues shown as sticks.

20

348

349 **METHODS**

350 **Protein expression and purification** PTg, a genetically detoxified pertussis toxin containing R9K and

351 E129G was produced from an engineered *Bp* BNA064 WCB strain [33]. This strain was cultured in

352 supplemented MSS medium at 35°C in shake flask then transferred to a fermenter. After 32-48 h of

353 growth, the culture supernatants were collected and processed with column chromatography to obtain a

354 purified PTg and qualified using validated quality control tests. Full-length antibody versions of hu11E6

355 and hu1B7 were produced with human IgG1/ kappa constant domains as previously described [31]. To

356 produce hu1B7 IgG and hu1B7 (hu1B7 S56A, Q61A, Q64A) IgG, FreeStyle 293 cells were co-

357 transfected with hu1B7 heavy chain and hu1B7 light chain, or hu1B7 heavy chain S56A, Q61A, Q64A

358 and hu1B7 light chain, respectively, using polyethylenimine (Polysciences). After 6 days, supernatant was

359 harvested and IgG was purified using Protein A resin (Thermo Fisher). Fabs were generated by addition

360 of 1:2000 wt/wt Endoproteinase Lys-C (Sigma) to hu11E6 IgG or hu1B7 IgG diluted to 1 mg/ml in PBS

361 and incubated overnight at 37 ºC. Subsequently, 1X Complete Protease Inhibitor Cocktail (Roche) was

362 added to each reaction. The hu1B7 and hu11E6 Fabs were purified using CaptureSelect IgG-CH1 affinity

363 resin (ThermoFisher) and further purified via size-exclusion chromatography using a Superdex 200

364 10/300 GL (Cytiva).

365 **Negative-stain electron microscopy** PTg at 0.04 mg/ml was mixed with a 2-fold molar excess of hu1B7

366 Fab and a 4-fold molar excess of hu11E6 Fab and allowed to bind for 20 minutes at room temperature in a

367 glass tube. The complex (4.8 µl) was added to CU-CF400 grids (Electron Microscopy Sciences) that had

368 been glow-discharged for 30s with using an Emitech K100X. The sample was then stained with NANO-

369 W methylamine tungstate stain solution (NanoProbes). Micrographs were collected (50) using a 200 kV

370 JEOL 2010F at a magnification of 120,000x (corresponding to 3.6 Å/pixel), at defocus values ranging

371 from -0.5 µm to -1.5 µm. CTF correction, particle picking, and 2D class-averaging were performed in

372 CryoSPARC.

373   **Cryo-electron microscopy** PTg (0.2 mg/ml in 20 mM Tris pH 7.5, 50 mM NaCl) was mixed with a 2-

374   fold molar excess of hu1B7 Fab and a 4-fold molar excess of hu11E6 Fab and allowed to bind for 20

375   minutes at room temperature in a glass tube. The sample was then mixed in a 1:1 ratio with 20 mM Tris

376   pH 7.5, 50 mM NaCl, 0.2% beta-octylglucoside resulting in a final concentration of 0.1 mg/ml PTg in 20

377   mM Tris pH 7.5, 50 mM NaCl, 0.1% β-octylglucoside. This sample (3 µl) was applied to an UltrAuFoil

378   holey gold grid (Electron Microscopy Sciences) that was previously plasma-cleaned for 4 minutes using a

379   Gatan Solarus 950 and then plunge-frozen using a Vitrobot Mark IV using +1 force, 3 second blot time,

380   100% humidity at 4 ºC. Movies (1,500) were collected at a magnification of 22,500x with a Titan Krios

381   and K3 detector, at a stage tilt of 30º. Motion correction, CTF estimation, particle picking, *ab-initio*

382   reconstruction, heterogeneous refinement, and homogeneous refinement were performed in CryoSPARC.

383   Map sharpening was performed using deepEMhancer. Model building and refinement were performed in

384   Coot, Phenix, and ISOLDE. Cryo-EM data collection and refinement statistics are in Table S1. For the

385   detergent screen, test cryo-EM images were taken in a 200 kV FEI Talos using an Ceta-M detector

386   (ThermoFisher) (no detergent, 0.1% amphipol) or a 300 kV Titan Krios using an Ceta-M detector

387   (ThermoFisher) (0.4% CHAPS, 0.04% fluoro-octyl maltoside, 0.1% β-octyl-glucoside).

388   **High-throughput glycan array** PTg at either 10 µM or 50 µM was incubated with 2-fold excess hu1B7

389   IgG (for detection) and either buffer or a 4-fold excess 11E6 Fab. The samples were then analyzed at the

390   National Center for Functional Glycomics (NCFG) using version 5.5 of the NCFG glycan array

391   containing 562 glycans. Each sample was analyzed in replicates of 6. The mean relative fluorescence unit

392   (RFU) values for each array were analyzed in the NCFG's GLAD software before being sorted into 3

393   categories: 'sialylated N-glycan', asialylated N-glycan' and 'other carbohydrate' and plotted in GraphPad

394   Prism 7.0.

395   **Binding assays** A high-binding 96-well ELISA plate (Costar) was incubated overnight at 4°C with 0.2

396   µg/mL PT (List Labs) in PBS, pH 7.4 or nothing (no coat). The plate was blocked with PBS-T-milk

397   (PBS, pH 7.4 with 0.05% Tween-20 and 5% non-fat dry milk) for 1 hr at 25°C. Antibodies diluted to 5

398   μg/mL in PBS-T-milk were added to both the PT-coated and uncoated wells of the plate in duplicate and

399   serially diluted 5-fold seven times. The antibodies were allowed to bind for 1 hr at 25°C. After washing

400   with PBS-T (PBS, pH 7.4, with 0.05% Tween-20), a 1:2000 dilution of goat-anti-human Fc-HRP

401   (Southern Biotech) in PBS-T-milk was added to each well and allowed to bind for 1 hr at 25°C. After

402   washing, the plate was developed with TMB substrate (Thermo Fisher Scientific) and quenched with 1 N

403   HCl. Absorbance was measured at 450 nm by using an Agilent BioTek Synergy H1 plate reader.

404   Measurements were fit to a 4-parameter logistic curve.

405   **CHO cell clustering assay** Enzymatically active PT (List Labs) was diluted to 10 pM in CHO-K1 culture

406   medium (high glucose DMEM with 10% fetal bovine serum and 1× penicillin and streptomycin). This PT

407   diluent was used to prepare dilutions of antibodies hu1B7, hu1B7 S57A/Q62A/Q65A, or human IgG1

408   isotype control. The human IgG1 isotype control was also prepared in CHO-K1 culture medium without

409   pertussis toxin (Isotype Control – no PT). The highest concentration of each antibody was 200 nM, with

410   seven additional 2-fold dilutions prepared in wells of a black-walled, clear bottom 96-well plate (Agilent).

411   The PT and antibody mixtures were incubated at 37°C for 30 min, then an equal volume of CHO-K1

412   culture medium with 10^4 CHO-K1 cells per well were added to the plate, diluting the pertussis toxin and

413   antibodies by 2-fold. The plate was allowed to incubate at 37°C for approximately 40 hr, then washed

414   with PBS+MgCa (PBS containing magnesium and calcium chloride, Sigma). PBS+MgCa with 1 μg/mL

415   Hoescht 33342 nuclear stain and 1 μM CFSE cytoplasmic stain was added to each well and the plate was

416   incubated at 37°C for 15 min. The plate was then washed one time with PBS+MgCa, one time with CHO-

417   K1 culture medium, two times with PBS+MgCa, then 50 uL of PBS+MgCa was added to each well for

418   imaging. The plates were imaged with a Cytation C10 plate imager using a 10x objective capturing

419   fluorescent images at 447 nm with 377 nm excitation (Hoescht 33342) and 525 nm with 469 nm

420   excitation (CFSE). Four images were captured and a montage created for each well. Masking was applied

421   to measure the area of non-CFSE fluorescent regions greater than 100 nm in diameter in each well. The

422   total empty area of each well was transformed to the Normalized Clustering Score by subtracting the

23

423 average empty area of the 100 nM Isotype Control – no PT from each empty area value and dividing the

424 result by the subtracted average empty area of the 100 nM Isotype Control with PT. These final data were

425 fit to [Inhibitor] vs. response equations using Prism (GraphPad).

426 **T cell activation assay** PBMCs from a healthy anonymized donor were isolated from 50 mL Leukopak

427 (Gulf Coast Regional Blood Center). Briefly, blood was diluted with PBS (1:1) and overlaid over Corning

428 Lymphocyte Separation Medium (Cat 25072CV). This was centrifuged for 30 min at 400g (no brake), the

429 lymphocyte layer was carefully removed, and residual red blood cells were lysed with RBC lysis buffer

430 (ThermoFisher Cat 00-4333-57). Cells were washed with PBS and cultured in 500 mL RPMI (Sigma Cat

431 R8758) with 50 mL heat inactivated FBS (Gibco Cat A52567-01), penicillin-streptomycin (Sigma Cat

432 P4458), 5 mL 100X non-essential amino acids (Gibco Cat 11140-050), 5 mL 100X GlutaMAX (Gibco

433 Cat 35050-061), 5 mL of 100 mM sodium pyruvate (Gibco 11360-070; PBMC media). PTg (1 µg/ml =

434 9.5 nM final concentration) was incubated with serially diluted Fab in 100 µl PBMC media for 1 hr at 37

435 °C, then combined with an equal volume of PBMCs (5×10^5 per well) and co-incubated overnight. Cells

436 were washed twice with 1% FBS in PBS (staining buffer) before incubation with 2.5 µg Fc block (BD

437 Biosciences Cat 564219) in staining buffer for 15 min at room temperature. Staining buffer containing

438 1:250 concentration of anti-CD3-PE, anti-CD69-APC, anti-CD4-FITC, and anti-CD8-BV421 (Biolegend

439 Cat 317308, 310910, 317408, 344747) was added directly to an equal volume of the Fc block and

440 incubated at room temperature for 20 minutes. Cells were washed twice with staining buffer before

441 collecting 10,000 events were collected per sample on a ThermoFisher Attune Flow Cytometer.

442 Sequential gating was performed based on size (FSC vs SSC), single cells (FSC-A vs FSC-H), the CD3-

443 expressing population and finally CD69-expression based on untreated negative controls. Data were

444 plotted using FlowJo 10.7.1 and Graphpad Prism 9.50; these data were fit to [inhibitor] vs. response

445 equations to determine IC_{50} values. Samples were run in duplicate with two experimental repeats per

446 donor.

REFERENCES

1. Yeung, K.H.T., et al., *An update of the global burden of pertussis in children younger than 5 years: a modelling study.* Lancet Infect Dis, 2017. **17**(9): p. 974-980.

2. Gregg, K.A. and T.J. Merkel, *Pertussis Toxin: A Key Component in Pertussis Vaccines?* Toxins (Basel), 2019. **11**(10).

3. Althouse, B.M. and S.V. Scarpino, *Asymptomatic transmission and the resurgence of Bordetella pertussis.* BMC Med, 2015. **13**: p. 146.

4. Klein, N.P., et al., *Waning Tdap Effectiveness in Adolescents.* Pediatrics, 2016. **137**(3): p. e20153326.

5. Smout, E., D. Mellon, and M. Rae, *Whooping cough rises sharply in UK and Europe.* BMJ, 2024. **385**: p. q736.

6. Hegerle, N. and N. Guiso, *Bordetella pertussis and pertactin-deficient clinical isolates: lessons for pertussis vaccines.* Expert Rev Vaccines, 2014. **13**(9): p. 1135-46.

7. Cherry, J.D., et al., *A search for serologic correlates of immunity to Bordetella pertussis cough illnesses.* Vaccine, 1998. **16**(20): p. 1901-6.

8. Storsaeter, J., et al., *Low levels of antipertussis antibodies plus lack of history of pertussis correlate with susceptibility after household exposure to Bordetella pertussis.* Vaccine, 2003. **21**(25-26): p. 3542-9.

9. Plotkin, S.A., *The pertussis problem.* Clin Infect Dis, 2014. **58**(6): p. 830-3.

10. Nguyen, A.W., et al., *Neutralization of pertussis toxin by a single antibody prevents clinical pertussis in neonatal baboons.* Science Advances, 2020. **6**: p. eaay9258.

11. Kapil, P., et al., *Maternal Vaccination with a Mono-component Pertussis Toxoid Vaccine is Sufficient to Protect Infants in a Baboon Model of Whooping Cough.* J Infect Dis, 2018. **217**(8): p. 1231-1236.

12. Bart, M.J., et al., *Complete Genome Sequences of 11 Bordetella pertussis Strains Representing the Pandemic ptxP3 Lineage.* Genome Announc, 2015. **3**(6): p. e01394-15.

13. Stein, P.E., et al., *The crystal structure of pertussis toxin.* Structure, 1994. **2**(1): p. 45-57.

14. Witvliet, M.H., et al., *Binding of pertussis toxin to eucaryotic cells and glycoproteins.* Infect Immun, 1989. **57**(11): p. 3324-30.

15. van't Wout, J., et al., *Role of carbohydrate recognition domains of pertussis toxin in adherence of Bordetella pertussis to human macrophages.* Infect Immun, 1992. **60**(8): p. 3303-8.

16. Plaut, R.D. and N.H. Carbonetti, *Retrograde transport of pertussis toxin in the mammalian cell.* Cell Microbiol, 2008. **10**(5): p. 1130-9.

17. Teter, K., *Intracellular Trafficking and Translocation of Pertussis Toxin.* Toxins (Basel), 2019. **11**(8).

18. Katada, T. and M. Ui, *Direct modification of the membrane adenylate cyclase system by islet-activating protein due to ADP-ribosylation of a membrane protein.* Proc Natl Acad Sci U S A, 1982. **79**(10): p. 3129-33.

19. Carbonetti, N.H., *Pertussis leukocytosis: mechanisms, clinical relevance and treatment.* Pathog Dis, 2016. **74**(7): p. pii: ftw087.

20. Bartoloni, A., et al., *Mapping of a protective epitope of pertussis toxin by in vitro refolding of recombinant fragments.* Nat Biotechnol, 1988. **6**: p. 709-712.

21. Sato, H., Y. Sato, and I. Ohishi, *Comparison of pertussis toxin (PT)-neutralizing activities and mouse-protective activities of anti-PT mouse monoclonal antibodies.* Infect Immun, 1991. **59**(10): p. 3832-5.

22. Sutherland, J.N. and J.A. Maynard, *Characterization of a key neutralizing epitope on pertussis toxin recognized by the monoclonal antibody 1B7.* Biochemistry, 2009. **48**(50): p. 11982-11993.

23. Acquaye-Seedah, E., et al., *Humanised monoclonal antibodies neutralise pertussis toxin by receptor blockade and reduced retrograde trafficking.* Cell Microbiol, 2018. **20**(12): p. e12948.

24.   Nencioni, L., et al., *Properties of pertussis toxin mutant PT-9K/129G after formaldehyde treatment.* Infect Immun, 1991. **59**(2): p. 625-30.

25.   Ibsen, P.H., *The effect of formaldehyde, hydrogen peroxide and genetic detoxification of pertussis toxin on epitope recognition by murine monoclonal antibodies.* Vaccine, 1996. **14**(5): p. 359-68.

26.   Sutherland, J.N., et al., *Antibodies recognizing protective pertussis toxin epitopes are preferentially elicited by natural infection versus acellular immunization.* Clin Vaccine Immunol, 2011. **18**(6): p. 954-62.

27.   Knuutila, A., et al., *Differences in epitope-specific antibodies to pertussis toxin after infection and acellular vaccinations.* Clin Transl Immunology, 2020. **9**(8): p. e1161.

28.   Di Tommaso, A., et al., *Acellular pertussis vaccines containing genetically detoxified pertussis toxin induce long-lasting humoral and cellular responses in adults.* Vaccine, 1997. **15**(11): p. 1218-24.

29.   Kamachi, K. and Y. Arakawa, *Development of safer pertussis DNA vaccine expressing non-toxic C180 polypeptide of pertussis toxin S1 subunit.* Vaccine, 2007. **25**(6): p. 1000-6.

30.   Wolf, M.A., et al., *Multivalent mRNA-DTP vaccines are immunogenic and provide protection from Bordetella pertussis challenge in mice.* NPJ Vaccines, 2024. **9**(1): p. 103.

31.   Nguyen, A.W., et al., *A cocktail of humanized anti-pertussis toxin antibodies limits disease in murine and baboon models of whooping cough.* Sci Transl Med, 2015. **7**(316): p. 316ra195.

32.   Wagner, E.K., et al., *Synergistic Neutralization of Pertussis Toxin by a Bispecific Antibody In Vitro and In Vivo.* Clin Vaccine Immunol, 2016. **23**(11): p. 851-862.

33.   Buasri, W., et al., *Construction of Bordetella pertussis strains with enhanced production of genetically-inactivated Pertussis Toxin and Pertactin by unmarked allelic exchange.* BMC Microbiol, 2012. **12**: p. 61.

34.   Russo, C.J. and L.A. Passmore, *Ultrastable gold substrates: Properties of a support for high-resolution electron cryomicroscopy of biological specimens.* J Struct Biol, 2016. **193**(1): p. 33-44.

35.   Stein, P.E., et al., *Structure of a pertussis toxin-sugar complex as a model for receptor binding.* Nat Struct Biol, 1994. **1**(9): p. 591-6.

36.   Millen, S.H., et al., *Identification and characterization of the carbohydrate ligands recognized by pertussis toxin via a glycan microarray and surface plasmon resonance.* Biochemistry, 2010. **49**(28): p. 5954-67.

37.   Schneider, O.D., A.A. Weiss, and W.E. Miller, *Pertussis toxin utilizes proximal components of the T-cell receptor complex to initiate signal transduction events in T cells.* Infect Immun, 2007. **75**(8): p. 4040-9.

38.   Kowalsky, C.A., et al., *Rapid fine conformational epitope mapping using comprehensive mutagenesis and deep sequencing.* J Biol Chem, 2015. **290**(44): p. 26457-70.

39.   Sakari, M., et al., *Crystal structures of pertussis toxin with NAD(+) and analogs provide structural insights into the mechanism of its cytosolic ADP-ribosylation activity.* J Biol Chem, 2022. **298**(5): p. 101892.

40.   Menetrey, J., et al., *Structural basis for the NAD-hydrolysis mechanism and the ARTT-loop plasticity of C3 exoenzymes.* Protein Sci, 2008. **17**(5): p. 878-86.

41.   Rossjohn, J., et al., *Aerolysin and pertussis toxin share a common receptor-binding domain.* EMBO J, 1997. **16**(12): p. 3426-34.

42.   Saukkonen, K., et al., *Pertussis toxin has eukaryotic-like carbohydrate recognition domains.* Proc Natl Acad Sci U S A, 1992. **89**(1): p. 118-22.

43.   Sato, H., et al., *Effect of monoclonal antibody to pertussis toxin on toxin activity.* Infect Immun, 1987. **55**(4): p. 909-15.

44.   Sato, H. and Y. Sato, *Protective activities in mice of monoclonal antibodies against pertussis toxin.* Infect Immun, 1990. **58**(10): p. 3369-74.

45.   Lee, S., et al., *Salmonella Typhoid Toxin PltB Subunit and Its Non-typhoidal Salmonella Ortholog Confer Differential Host Adaptation and Virulence.* Cell Host Microbe, 2020. **27**(6): p. 937-949 e6.

46.   Rudolph, M.J., et al., *Structural Analysis of Toxin-Neutralizing, Single-Domain Antibodies that Bridge Ricin's A-B Subunit Interface.* J Mol Biol, 2021. **433**(15): p. 167086.

47.   Mukhopadhyay, S. and A.D. Linstedt, *Manganese blocks intracellular trafficking of Shiga toxin and protects against Shiga toxicosis.* Science, 2012. **335**(6066): p. 332-5.

48.   Nowakowska-Golacka, J., et al., *Toxins Utilize the Endoplasmic Reticulum-Associated Protein Degradation Pathway in Their Intoxication Process.* Int J Mol Sci, 2019. **20**(6).

49.   Pitisuttithum, P., et al., *Antibody persistence after vaccination of adolescents with monovalent and combined acellular pertussis vaccines containing genetically inactivated pertussis toxin: a phase 2/3 randomised, controlled, non-inferiority trial.* Lancet Infect Dis, 2018. **18**(11): p. 1260-1268.

50.   Puthanakit, T., et al., *A phase 2 randomized controlled dose-ranging trial of recombinant pertussis booster vaccines containing genetically inactivated pertussis toxin in pregnant women.* Vaccine, 2023. **41**(31): p. 4541-4553.

51.   Gomez, S.R., et al., *Development of a carbohydrate binding assay for the B-oligomer of pertussis toxin and toxoid.* Anal Biochem, 2006. **356**(2): p. 244-53.

52.   Ausar, S.F., et al., *Genetically detoxified pertussis toxin displays near identical structure to its wild-type and exhibits robust immunogenicity.* Commun Biol, 2020. **3**(1): p. 427.

`